

## Research Article

# On $J/\psi$ and $\Upsilon$ Transverse Momentum Distributions in High Energy Collisions

**Bao-Chun Li, Ting Bai, Yuan-Yuan Guo, and Fu-Hu Liu**

*Department of Physics, Shanxi University, Taiyuan, Shanxi 030006, China*

Correspondence should be addressed to Bao-Chun Li; libc2010@163.com

Received 27 December 2016; Revised 14 March 2017; Accepted 26 March 2017; Published 18 May 2017

Academic Editor: Chao-Qiang Geng

Copyright © 2017 Bao-Chun Li et al. This is an open access article distributed under the Creative Commons Attribution License, which permits unrestricted use, distribution, and reproduction in any medium, provided the original work is properly cited. The publication of this article was funded by SCOAP<sup>3</sup>.

The transverse momentum distributions of final-state particles are very important for high energy collision physics. In this work, we investigate  $J/\psi$  and  $\Upsilon$  meson distributions in the framework of a particle-production source, where Tsallis statistics are consistently incorporated. The results are in good agreement with the experimental data in p-p and p-Pb collisions at LHC energies. The temperature of the emission source and the nonequilibrium degree of the collision system are extracted.

## 1. Introduction

The investigation of nuclear matter at high energy densities is the main purpose of Relativistic Heavy Ion Collider (RHIC) and Large Hadron Collider (LHC) [1–7]. As a new matter state, quark-gluon plasma (QGP) is a thermalized system, which consists of strongly coupled quarks and gluons in a limited region. The suppression of  $J/\psi$  meson with respect to proton-proton (p-p) collisions is regarded as a distinctive signature of the QGP formation and brings valuable insight into properties of the nuclear matter. In proton-nucleus (p-A) collisions, the prompt  $J/\psi$  meson suppression has also been observed at large rapidity [8]. The low-viscosity QGP may be created in the small system,  $^3\text{He} + \text{Au}$  collisions [9]. The heavy quarkonium production can be suppressed by the suppression cold-nuclear-matter (CNM) effects, such as nuclear absorption, nuclear shadowing (antishadowing), and parton energy loss.

The transverse momentum  $p_T$  spectra of identified particles produced in the collisions are a vital research for physicists. Now, different models have been suggested to describe the  $p_T$  distributions of the final-state particles in high energy collisions [10–13], such as Boltzmann distribution, Rayleigh distribution, Erlang distribution, the multisource thermal model, and Tsallis statistics. Different phenomenological models of initial coherent multiple interactions

and particle transport have been proposed to discuss the particle production in high energy collisions. Tsallis statistics can deal with nonequilibrated complex systems in condensed-matter research [14]. It is developed to describe the particle production in recent years [15–24].

In our previous work [12], the temperature information was understood indirectly by an excitation degree. We have obtained the emission source location dependence of the exciting degree specifically. In this paper, the temperature of the emission source is given directly by combining a picture of the particle-production source with Tsallis statistics. We discuss the transverse momentum distributions of  $J/\psi$  in p-p collisions at  $\sqrt{s_{\text{NN}}} = 7$  TeV,  $\sqrt{s_{\text{NN}}} = 8$  TeV, and  $\sqrt{s_{\text{NN}}} = 13$  TeV and p-Pb collisions at  $\sqrt{s_{\text{NN}}} = 5$  TeV. And the  $\Upsilon$  distributions in p-p collisions at  $\sqrt{s_{\text{NN}}} = 8$  TeV are also taken into account for comparison.

## 2. Tsallis Statistics in an Emission Source

According to the multisource thermal model [12] and the nuclear geometry picture, at the initial stage of the collision, two cylinder-shaped groups are formed along the beam direction. In the laboratory reference frame, it is assumed that the projectile cylinder is at the positive  $y$  space and the target cylinder is at the negative  $y$  space. The cylinders are

not a real shape and are understood to be a rapidity range of the emission source. The projectile and target cylinders can be regarded as an emission source with a rapidity width. The observed particles are emitted from the emission source.

With Tsallis statistics' success in dealing with nonequilibrium complex systems in condensed-matter research [14], it has been used to understand the particle production in high energy physics. In order to describe the transverse momentum spectra in high energy collisions, several versions of Tsallis distribution are proposed [15–24]. Recently, an improved form of the Tsallis distribution was proposed [18–20] and can meet the thermodynamic consistency. The meson number [16, 17] is given by

$$N = gV \int \frac{d^3 p}{(2\pi)^3} \left[ 1 + (q-1) \frac{E - \mu}{T} \right]^{1/(1-q)}, \quad (1)$$

where  $g$ ,  $V$ ,  $p$ ,  $E$ , and  $\mu$  are the degeneracy factor, the volume, the momentum, the energy, and the chemical potential, respectively. The parameter  $T$  is the temperature of the emission source and the parameter  $q$  is the nonequilibrium degree. Generally,  $q$  is greater than 1 and is close to 1. The corresponding momentum distribution is given by

$$E \frac{d^3 N}{d^3 p} = gVE \frac{1}{(2\pi)^3} \left[ 1 + (q-1) \frac{E - \mu}{T} \right]^{1/(1-q)}. \quad (2)$$

Then, the transverse momentum distribution is

$$\begin{aligned} & \frac{d^2 N}{p_T dy dp_T} \\ &= gV \frac{m_T \cosh y}{(2\pi)^2} \left[ 1 + (q-1) \frac{m_T \cosh y - \mu}{T} \right]^{1/(1-q)}. \end{aligned} \quad (3)$$

When the chemical potential is neglected, at midrapidity  $y = 0$ , the  $p_T$  distribution is

$$\frac{d^2 N}{p_T dy dp_T} = \frac{gV m_T}{(2\pi)^2} \left[ 1 + (q-1) \frac{m_T}{T} \right]^{1/(1-q)}. \quad (4)$$

It is worth noting that the distribution function of  $p_T$  is only the distribution of mesons emitted from an emission point at  $y = 0$  in the emission source, not the final-state distribution due to the nonzero rapidity width of the emission source. By summing the contributions of all emission points, the transverse momentum  $p_T$  distribution is rewritten as

$$\begin{aligned} & \frac{dN}{p_T dp_T} \\ &= c \int_{y_{\min}}^{y_{\max}} \cosh y dy m_T \left[ 1 + (q-1) \frac{m_T \cosh y}{T} \right]^{1/(1-q)}, \end{aligned} \quad (5)$$

where  $c = gV/(2\pi)^2$  is a normalize constant and  $y_{\max}$  and  $y_{\min}$  are the maximum and minimum values of the observed rapidity.

TABLE 1: Values of  $T$  and  $q$  used in Figures 1-2.

Figure	$y$ bins	$T$ (GeV)	$q$	$\chi^2/\text{dof}$
Figure 1(a)	$2.0 < y < 2.5$	0.845	1.018	0.926
	$2.5 < y < 3.0$	0.833	1.020	1.052
	$3.0 < y < 3.5$	0.801	1.024	1.078
	$3.5 < y < 4.0$	0.789	1.021	1.127
Figure 1(b)	$4.0 < y < 4.5$	0.755	1.015	1.074
	$2.0 < y < 2.5$	0.863	1.034	1.244
	$2.5 < y < 3.0$	0.850	1.033	1.310
	$3.0 < y < 3.5$	0.838	1.032	1.317
Figure 1(c)	$3.5 < y < 4.0$	0.783	1.028	1.293
	$4.0 < y < 4.5$	0.725	1.026	1.280
	$2.0 < y < 2.5$	0.950	1.002	1.302
	$2.5 < y < 3.0$	0.900	1.011	1.208
Figure 1(d)	$3.0 < y < 3.5$	0.875	1.012	1.226
	$3.5 < y < 4.0$	0.867	1.003	1.251
	$4.0 < y < 4.5$	0.826	1.001	1.295
	$2.0 < y < 2.5$	0.845	1.020	1.150
Figure 2(a)	$2.5 < y < 3.0$	0.840	1.017	1.174
	$3.0 < y < 3.5$	0.836	1.016	1.127
	$3.5 < y < 4.0$	0.829	1.010	1.203
	$4.0 < y < 4.5$	0.802	1.001	1.192
Figure 2(b)	$2.0 < y < 2.5$	0.882	1.013	1.239
	$2.5 < y < 3.0$	0.880	1.013	1.282
	$3.0 < y < 3.5$	0.876	1.011	1.255
	$3.5 < y < 4.0$	0.873	1.008	1.291
Figure 2(a)	$4.0 < y < 4.5$	0.866	1.003	1.385
	$2.0 < y < 2.5$	0.885	1.038	1.103
	$2.5 < y < 3.0$	0.880	1.036	1.055
	$3.0 < y < 3.5$	0.874	1.031	1.346
Figure 2(b)	$3.5 < y < 4.0$	0.830	1.030	1.174
	$4.0 < y < 4.5$	0.805	1.029	1.230

### 3. Transverse Momentum Spectra and Discussions

Figure 1 shows the double-differential cross section  $d^2\sigma/dp_T dy$  of  $J/\psi$  mesons in p-p collisions at  $\sqrt{s_{NN}} = 7$  TeV. Figures 1(a), 1(b), 1(c), and 1(d) present prompt  $J/\psi$  with no polarisation,  $J/\psi$  from  $b$  with no polarisation, prompt  $J/\psi$  with full transverse polarisation, and prompt  $J/\psi$  with full longitudinal polarisation, respectively. The experimental data in  $y$  bins are from the LHCb Collaboration [25]. The solid lines indicate our model results, which are in good agreement with the experimental data in all rapidity ranges. The parameters  $T$  and  $q$  taken for the calculation are listed in Table 1. In different rapidity ranges, the values of the temperature  $T$  are different and decrease with increasing the rapidity bins in all four figures of Figure 1. The closer the emission source is to the center  $y = 0$ , the larger the excitation degree is. The values of  $q$  do not change regularly with the rapidity bins.

Figure 2 presents the double-differential cross section  $d^2\sigma/dp_T dy$  of  $J/\psi$  mesons in p-p collisions at  $\sqrt{s_{NN}} = 8$  TeV.

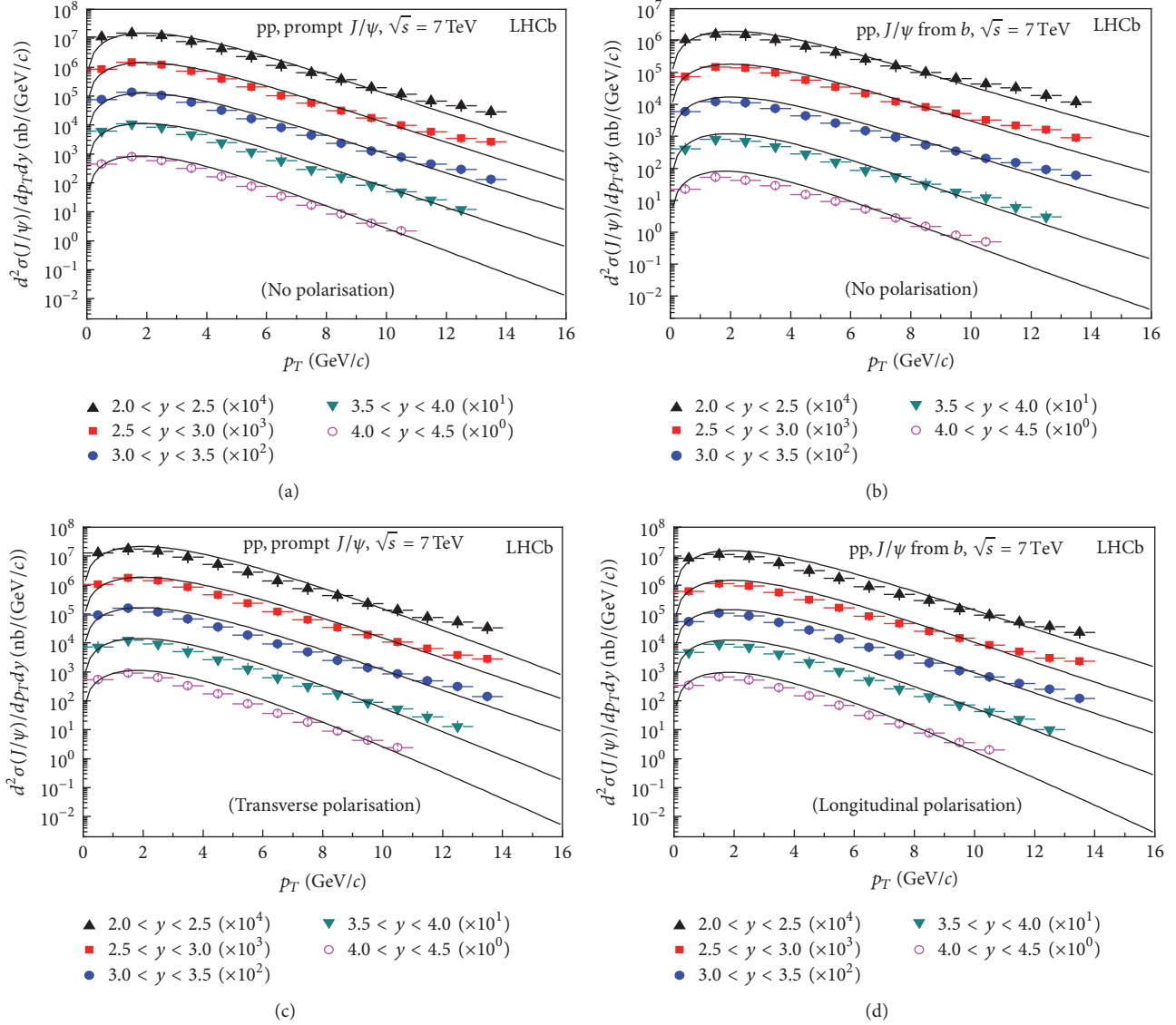


FIGURE 1: Double-differential cross section  $d^2\sigma/dp_T dy$  as a function of  $p_T$  in bins of  $y$  for (a) prompt  $J/\psi$  with no polarisation, (b)  $J/\psi$  from  $b$  with no polarisation, (c) prompt  $J/\psi$  with full transverse polarisation, and (d) prompt  $J/\psi$  with full longitudinal polarisation in p-p collisions at  $\sqrt{s_{NN}} = 7$  TeV. The symbols indicate the experimental data of the LHCb Collaboration [15]. The solid lines indicate our theoretical calculations.

Figures 2(a) and 2(b) are prompt  $J/\psi$  and  $J/\psi$  from  $b$ , respectively. Figure 3 presents the double-differential cross section  $B^{iS} d^2\sigma^{iS}/dp_T dy$  of  $Y$  mesons in the same collision, where  $i = 1, 2, \text{ and } 3$  correspond to  $Y(1S), Y(2S), \text{ and } Y(3S)$  mesons, respectively, and  $B$  is the dimuon branching fraction. The experimental data are from [26]. The symbols and lines represent the same meanings as those in Figure 1. The model results are also in agreement with the experiment data. The parameters  $T$  and  $q$  for the calculation are listed in Tables 1 and 2. The freeze-out temperature  $T$  also decreases with increasing the rapidity bins for both  $J/\psi$  and  $Y$ . In the same  $y$  ranges, the  $T$  values are smaller for  $Y$  than that for  $J/\psi$ . For  $J/\psi$ , the  $T$  values are generally larger than that at  $\sqrt{s_{NN}} = 7$  TeV.  $q$  for  $J/\psi$  and for  $Y$  are 1.003–1.038 and 1.170–1.127,

respectively. At  $p_T > 12$  GeV, the agreement is not very good in Figures 1-2 and the  $\chi^2/\text{dof}$  values are in the range 0.926–1.385.

Figure 4 presents the double-differential cross section  $d^2\sigma/dp_T dy$  of  $J/\psi$  mesons produced in p-p collisions at  $\sqrt{s_{NN}} = 13$  TeV. The experimental data are from [27]. The symbols and lines represent the same meanings as those in Figure 1. The results are also in agreement with the experiment data. The  $T$  and  $q$  values taken for the calculation are listed in Table 2. The temperature  $T$  decreases with increasing the rapidity bins. As the emission source draws closer to the center, the excitation degree gets larger. The  $T$  values are larger than that at  $\sqrt{s_{NN}} = 8$  TeV in the same  $y$  range. The  $q$  behavior is similar to that in Figures 1 and 2.

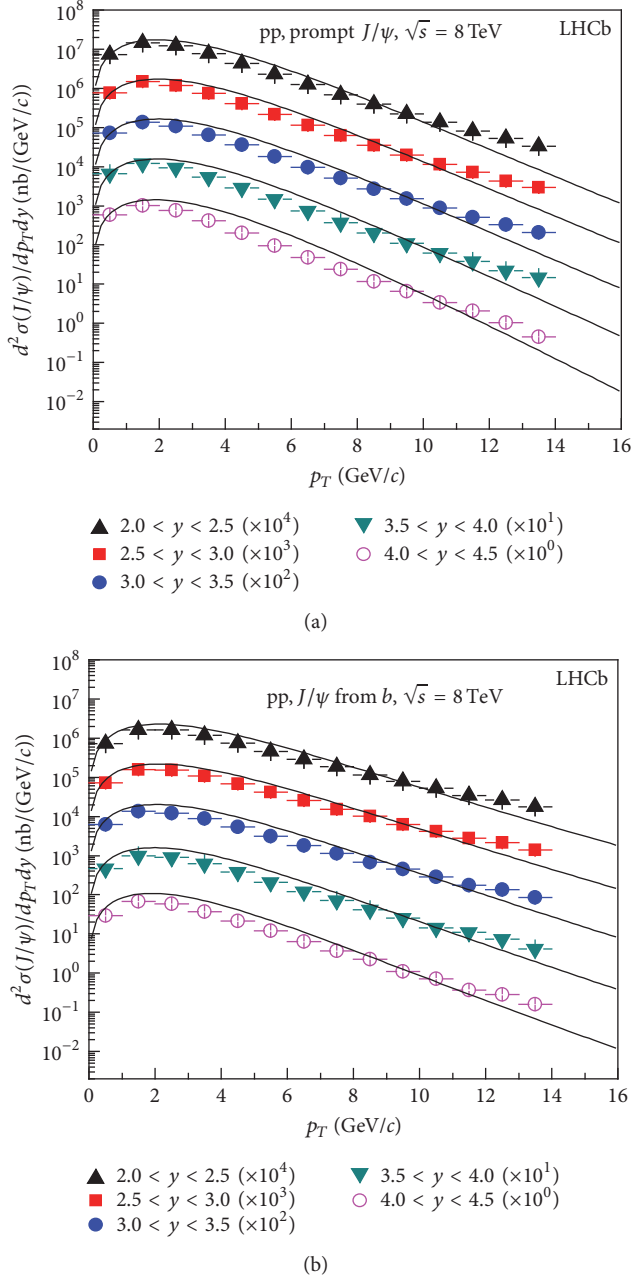


FIGURE 2: Double-differential cross section  $d^2\sigma/dp_T dy$  as a function of  $p_T$  in bins of  $y$  for (a) prompt  $J/\psi$  and (b)  $J/\psi$  from  $b$  in p-p collisions at  $\sqrt{s_{NN}} = 8$  TeV. The symbols indicate the experimental data of the LHCb Collaboration [25]. The solid lines indicate our theoretical calculations.

For comparison, Figure 5 presents the double-differential cross section  $d^2\sigma/dp_T dy$  of  $J/\psi$  mesons in p-Pb collisions at  $\sqrt{s_{NN}} = 5$  TeV. The experimental data are from [8]. The symbols and lines represent the same meanings as those in Figure 1. The results are also in agreement with the experiment data. The parameters  $T$  and  $q$  taken for the calculation are listed in Table 2. The temperature  $T$  of the emission source decreases with increasing the rapidity bins. The  $q$  values are between 1.031 and 1.065. In the calculation, the least-square-fitting testing provides a statistical indication

TABLE 2: Values of  $T$  and  $q$  used in Figures 3–5.

Figure	$y$ bins	$T$	$q$	$\chi^2/\text{dof}$
Figure 3(a)	$2.0 < y < 2.5$	0.744	1.138	0.152
	$2.5 < y < 3.0$	0.734	1.132	0.124
	$3.0 < y < 3.5$	0.728	1.130	0.160
	$3.5 < y < 4.0$	0.670	1.132	0.128
	$4.0 < y < 4.5$	0.610	1.127	0.216
Figure 3(b)	$2.0 < y < 2.5$	0.795	1.170	0.280
	$2.5 < y < 3.0$	0.790	1.168	0.356
	$3.0 < y < 3.5$	0.788	1.165	0.209
	$3.5 < y < 4.0$	0.784	1.151	0.375
	$4.0 < y < 4.5$	0.770	1.133	0.481
Figure 3(c)	$2.0 < y < 2.5$	0.703	1.169	0.415
	$2.5 < y < 3.0$	0.688	1.168	0.225
	$3.0 < y < 3.5$	0.684	1.167	0.233
	$3.5 < y < 4.0$	0.680	1.157	0.410
	$4.0 < y < 4.5$	0.605	1.131	0.504
Figure 4(a)	$2.0 < y < 2.5$	0.962	1.035	0.429
	$2.5 < y < 3.0$	0.940	1.034	0.418
	$3.0 < y < 3.5$	0.928	1.033	0.371
	$3.5 < y < 4.0$	0.902	1.032	0.273
	$4.0 < y < 4.5$	0.882	1.031	0.350
Figure 4(b)	$2.0 < y < 2.5$	0.988	1.065	0.182
	$2.5 < y < 3.0$	0.964	1.063	0.254
	$3.0 < y < 3.5$	0.936	1.060	0.261
	$3.5 < y < 4.0$	0.910	1.057	0.270
	$4.0 < y < 4.5$	0.856	1.054	0.315
Figure 5(a)	$1.5 < y < 2.0$	0.792	1.040	0.436
	$2.0 < y < 2.5$	0.786	1.037	0.304
	$2.5 < y < 3.0$	0.784	1.036	0.391
	$3.0 < y < 3.5$	0.782	1.033	0.452
	$3.5 < y < 4.0$	0.780	1.025	0.526
Figure 5(b)	$1.5 < y < 2.0$	0.843	1.053	0.170
	$2.0 < y < 2.5$	0.840	1.050	0.225
	$2.5 < y < 3.0$	0.838	1.048	0.303
	$3.0 < y < 3.5$	0.836	1.041	0.518
	$3.5 < y < 4.0$	0.822	1.026	0.531

of the most probable values of the two parameters. The values of  $\chi^2/\text{dof}$  corresponding to the curves in Figures 1–5 are given in Tables 1 and 2. By the comparison between the model results and experimental data, we obtain the temperature of the emission source. For  $J/\psi$  particles in the same  $y$  bins, the temperature increases with increasing the collision energy. In p-p collision at  $\sqrt{s_{NN}} = 8$  TeV, the temperature is smaller for  $\Upsilon$  than that for  $J/\psi$  in the same  $y$  ranges.

## 4. Conclusions

Final-state particle production in high energy collisions has attracted much attention since the attempt has been made to understand the properties of strongly coupled QGP. Thermal-statistical models have been successful in describing particle

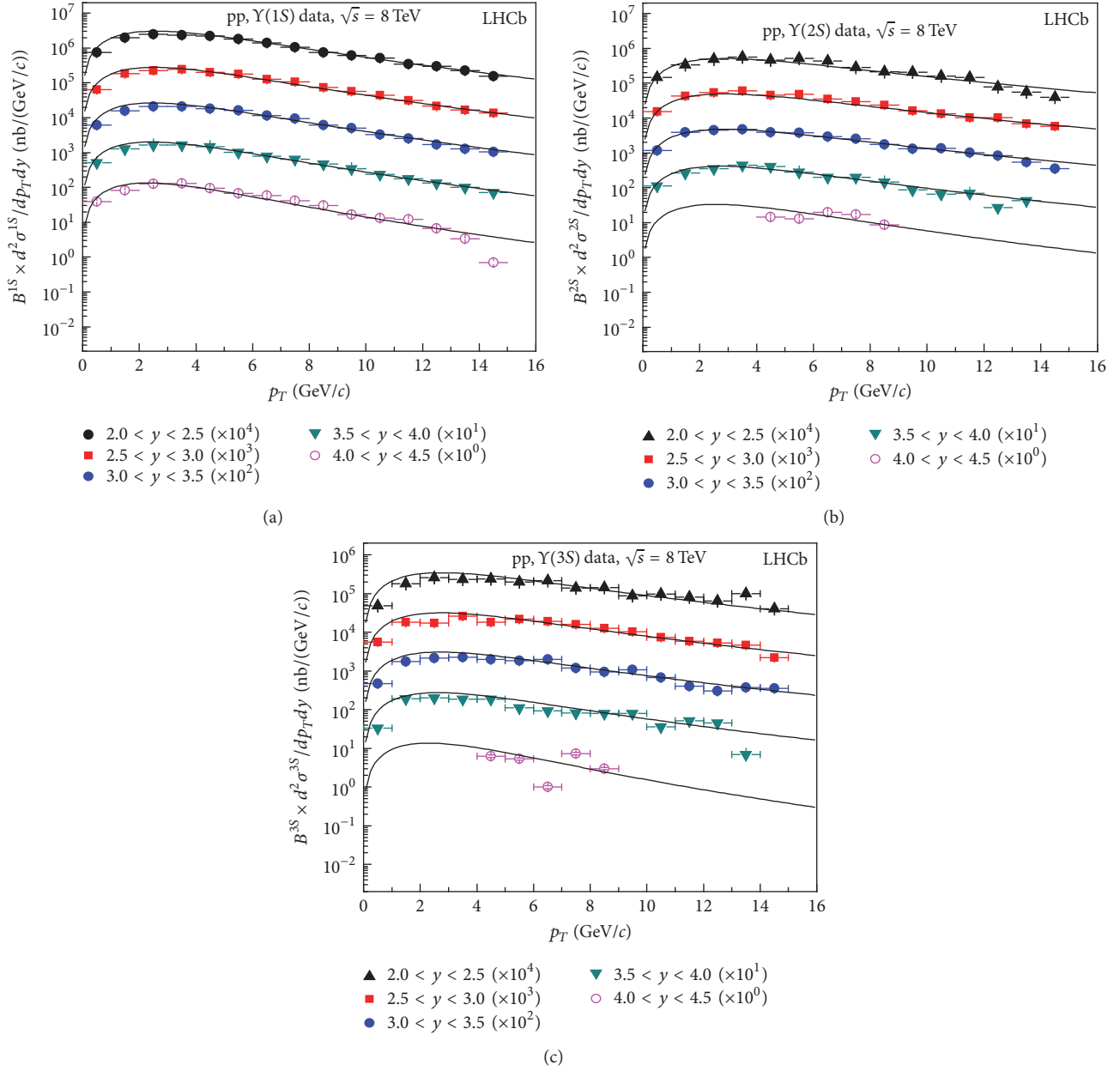


FIGURE 3: Double-differential cross section  $d^2\sigma/dp_T dy$  as a function of  $p_T$  in bins of  $y$  for (a) Y(1S), (b) Y(2S), and (c) Y(3S) mesons in p-p collision at  $\sqrt{s_{NN}} = 8$  TeV. The symbols indicate the experimental data of the LHCb Collaboration [25]. The solid lines indicate our theoretical calculations.

yields in various systems at different energies. The emission source temperature is very important for understanding the matter evolution in p-p collisions at high energy. In the rapidity space, different final-state particles are emitted from different positions due to stronger longitudinal flow. In our previous work [12], we have studied the transverse momentum spectra of strange particles produced in A-A collisions at  $\sqrt{s_{NN}} = 62.4$  and 200 GeV in the improved fireball model. The temperature  $T$  of the emission source was characterized indirectly by the excitation degree, which varies with location in the cylinder. In the present work, we can directly extract the specific temperature by Tsallis statistics.

In this work, we have embedded consistently the Tsallis statistics into the picture of the multisource thermal model for descriptions of the transverse momentum spectra of  $J/\psi$  and  $\Upsilon$  mesons produced in pp and p-Pb collisions over an energy range from 5 to 13 TeV, with different rapidity intervals. In most cases, the model results are in good agreement with the experimental data of the LHCb Collaboration. The agreement is not very good at  $p_T > 12$  GeV in Figures 1-2. In other collisions, the maximum  $\chi^2/\text{dof}$  value is 0.531 and the minimum value is 0.124. By comparing with the experimental data, the temperature of the emission source and the nonequilibrium degree of the collision system are extracted.

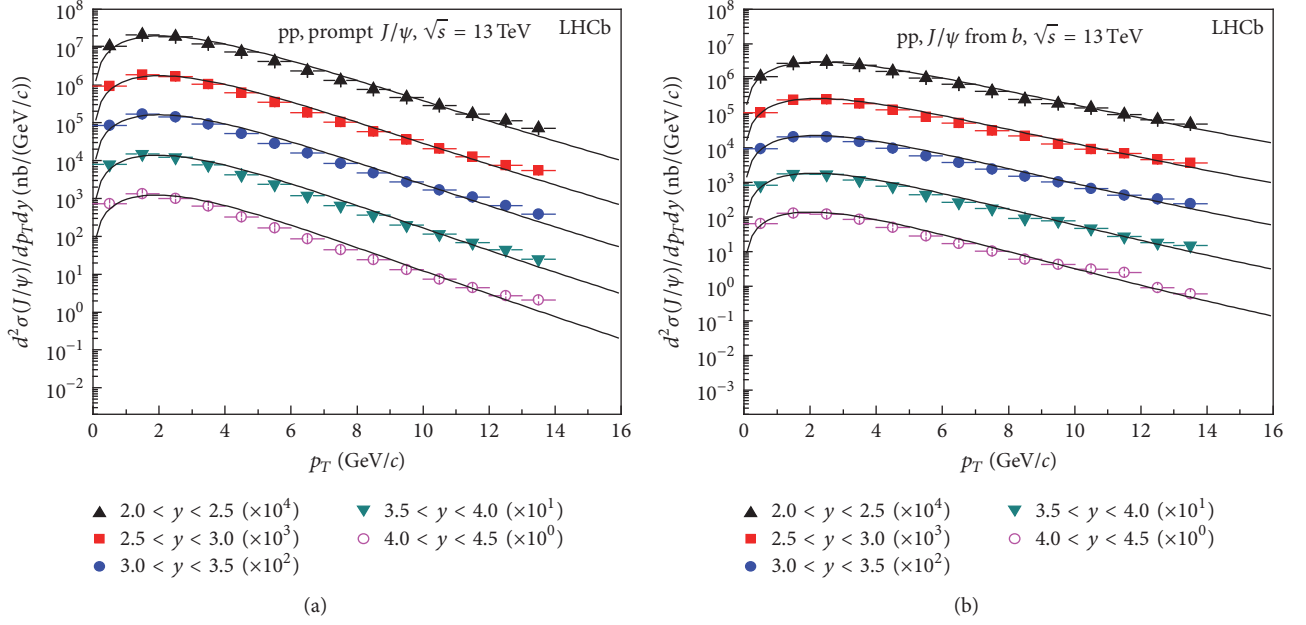


FIGURE 4: Same as Figure 2, but for  $\sqrt{s_{NN}} = 13$  TeV. The experimental data are taken from the LHCb Collaboration [26].

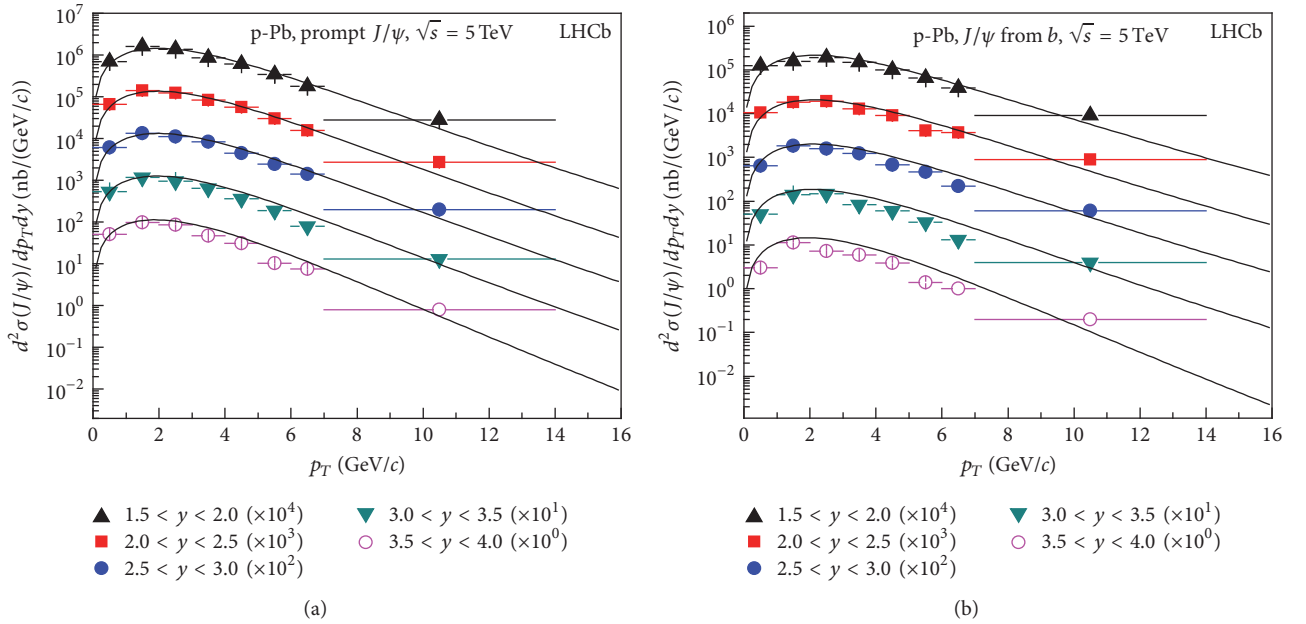


FIGURE 5: Same as Figure 2, but for p-Pb collisions at  $\sqrt{s_{NN}} = 5$  TeV. The experimental data are taken from the LHCb Collaboration [27].

In p-p and p-Pb collisions, the temperature decreases with increasing the rapidity bins. The closer the emission source is to the  $y$  center, the larger the excitation degree is. For  $J/\psi$  particles in the same  $y$  bins, the temperature  $T$  increases with increasing the collision energy. So, the excitation degree of the emission source also increases with increasing the collision energy. In p-p collision at  $\sqrt{s_{NN}} = 8$  TeV, the temperature is smaller for  $Y$  than that for  $J/\psi$  in the same  $y$  ranges. The parameter  $q$  does not change significantly, which means the collision system is not very unstable.

In summary, the transverse momentum spectra of  $J/\psi$  and  $Y$  mesons produced in p-p and p-Pb collisions at high energies have been studied by combining a picture of the particle-production source with Tsallis statistics. The model results are compared with the experimental data of the LHCb Collaboration. Our investigations show the improved model is successful in the description of the transverse momentum distributions. At the same time, it can offer the temperature of the emission source and the information about the nonequilibrium degree in the collisions.

## Conflicts of Interest

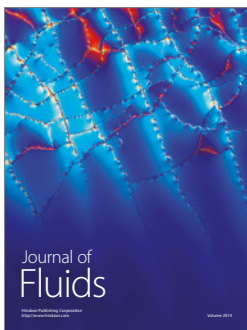
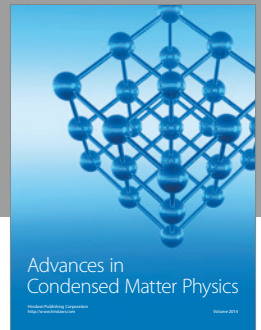
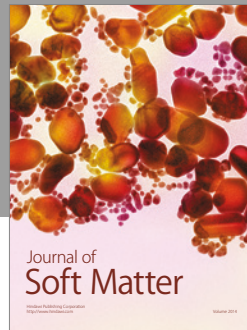
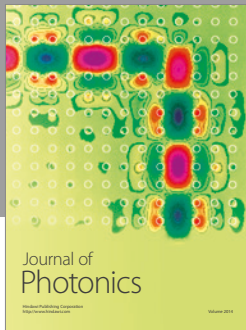
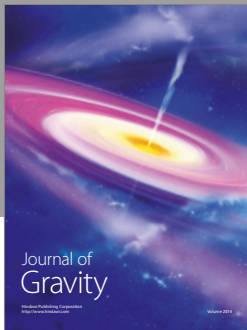
The authors declare that they have no conflicts of interest.

## Acknowledgments

This work is supported by the National Natural Science Foundation of China under Grant nos. 11575103, 11247250, and 10975095, the National Fundamental Fund of Personnel Training under Grant no. J1103210, and the Shanxi Provincial Natural Science Foundation under Grant no. 2013021006.

## References

- [1] K. Aamodt, B. Abelev, and A. A. Quintana et al., “Elliptic flow of charged particles in pb-pb collisions at  $\sqrt{s_{NN}} = 2.76$  TeV,” *Physical Review Letters*, vol. 105, Article ID 252302, 2010.
- [2] A. Adare, S. Afanasiev, and C. Aidala et al., “Elliptic and hexadecapole flow of charged hadrons in Au+Au collisions at  $\sqrt{s_{NN}} = 200$  GeV,” *Physical Review Letters*, vol. 105, Article ID 062301, 2010.
- [3] S. Uddin, R. A. Bhat, I.-U. Bashir, W. Bashir, and J. S. Ahmad, “Systematic of particle thermal freeze-out in a hadronic fireball at RHIC,” *Nuclear Physics A*, vol. 934, no. 1, pp. 121–132, 2015.
- [4] V. Khachatryan et al., “Multiplicity and rapidity dependence of strange hadron production in pp, pPb, and PbPb collisions at the LHC.”
- [5] M. Petráň, J. Letessier, V. Petráček, and J. Rafelski, “Hadron production and quark-gluon plasma hadronization in Pb-Pb collisions at  $\sqrt{s_{NN}} = 2.76$  TeV,” *Physical Review C*, vol. 88, Article ID 034907, 2013.
- [6] N. B. Chang and G. Y. Qin, “Full jet evolution in quark-gluon plasma and nuclear modification of jet production and jet shape in Pb+Pb collisions at 2.76A TeV at the CERN large hadron collider,” *Physical Review C*, vol. 94, Article ID 024902, 2016.
- [7] M. Nahrgang, J. Aichelin, S. Bass, P. B. Gossiaux, and K. Werner, “Heavy-flavor observables at RHIC and LHC,” *Nuclear Physics A*, vol. 931, pp. 575–580, 2014.
- [8] B. Adeva, M. Adinolfi, and R. Aaij et al., “Study of  $J/\psi$  production and cold nuclear matter effects in pPb collisions at  $\sqrt{s_{NN}} = 5$  TeV,” *Journal of High Energy Physics*, vol. 2, article 072, 2014.
- [9] A. Adare, S. Afanasiev, and C. Aidala et al., “Measurements of elliptic and triangular flow in high-multiplicity  $^3\text{He}+\text{Au}$  collisions at  $\sqrt{s_{NN}} = 200$  GeV,” *Physical Review Letters*, vol. 115, Article ID 142301, 2015.
- [10] P. Braun-Munzinger, D. Magestro, K. Redlich, and J. Stachel, “Hadron production in Au-Au collisions at RHIC,” *Physics Letters B*, vol. 518, p. 41, 2001.
- [11] J. Rafelski and J. Letessier, “Testing limits of statistical hadronization,” *Nuclear Physics A*, vol. 715, p. 98, 2003.
- [12] B. C. Li, Y. Y. Fu, L. L. Wang, E. Q. Wang, and F. H. Liu, “Transverse momentum distributions of strange hadrons produced in nucleus–nucleus collisions at  $\sqrt{s_{NN}} = 62.4$  and 200 GeV,” *Journal of Physics G*, vol. 39, Article ID 025009, 2012.
- [13] G. Wolschin, “Beyond the thermal model in relativistic heavy-ion collisions,” *Physical Review C*, vol. 94, Article ID 024911, 2016.
- [14] C. Tsallis, “Possible generalization of boltzmann-gibbs statistics,” *Journal of Statistical Physics*, vol. 52, p. 479, 1988.
- [15] M. Shao, L. Yi, Z. Tang, H. Chen, C. Li, and Z. Xu, “Examination of the species and beam energy dependence of particle spectra using tsallis statistics,” *Journal of Physics G*, vol. 37, Article ID 085104, 2010.
- [16] Z. Tang, Y. Xu, L. Ruan, G. van Buren, F. Wang, and Z. Xu, “Spectra and radial flow in relativistic heavy ion collisions with Tsallis statistics in a blast-wave description,” *Physical Review C*, vol. 79, Article ID 051901, 2009.
- [17] J. Cleymans, G. I. Lykasov, A. S. Parvan, A. S. Sorin, O. V. Teryaev, and D. Worku, “Systematic properties of the Tsallis distribution: Energy dependence of parameters in high energy p-p collisions,” *Physics Letters B*, vol. 723, no. 4-5, pp. 351–354, 2013.
- [18] J. Cleymans and D. Worku, “The Tsallis distribution in proton-proton collisions at  $\sqrt{s} = 0.9$  TeV at the LHC,” *Journal of Physics G*, vol. 39, Article ID 025006, 2012.
- [19] J. Cleymans and D. Worku, “Relativistic thermodynamics: transverse momentum distributions in high-energy physics,” *The European Physical Journal A*, vol. 48, article 160, 2012.
- [20] A. Deppman, “Properties of hadronic systems according to the nonextensive self-consistent thermodynamics,” *Journal of Physics G*, vol. 41, Article ID 055108, 2014.
- [21] A. Adare, S. Afanasiev, and C. Aidala et al., “Measurement of neutral mesons in p + p collisions at  $\sqrt{s} = 200$  GeV and scaling properties of hadron production,” *Physical Review D*, vol. 83, Article ID 052004, 2011.
- [22] K. Aamodt, N. Abel, and U. Abeysekara et al., “Transverse momentum spectra of charged particles in proton-proton collisions at  $\sqrt{s} = 900$  GeV with ALICE at the LHC,” *Physics Letters B*, vol. 693, p. 53, 2010.
- [23] V. Khachatryan, A. M. Sirunyan, and A. Tumasyan et al., “Transverse-momentum and pseudorapidity distributions of charged hadrons in pp collisions at  $\sqrt{s} = 0.9$  and 2.36 TeV,” *Journal of High Energy Physics*, vol. 2, article 41, 2010.
- [24] V. Khachatryan, A. M. Sirunyan, A. Tumasyan, and W. Adam, “Transverse-momentum and pseudorapidity distributions of charged hadrons in pp collisions at  $\sqrt{s} = 7$  TeV,” *Physical Review Letters*, vol. 105, Article ID 022002, 2010.
- [25] R. Aaij, B. Adeva, and M. Adinolfi, “Measurement of  $J/\psi$  production in pp collisions at  $\sqrt{s} = 7$  TeV,” *The European Physical Journal C*, vol. 71, article 1645, 2011.
- [26] R. Aaij, C. A. Beteta, B. Adeva, M. Adinolfi, and C. Adrover et al., “Production of  $J/\psi$  and Upsilon mesons in pp collisions at  $\sqrt{s} = 8$  TeV,” *Journal of High Energy Physics*, vol. 06, article 064, 2013.
- [27] R. Aaij, B. Adeva, M. Adinolfi, A. Affolder, and Z. Ajaltouni, “Measurement of forward  $J/\psi$  production cross-sections in pp collisions at  $\sqrt{s} = 13$  TeV,” *Journal of High Energy Physics*, vol. 10, article 172, 2015.



**Hindawi**

Submit your manuscripts at  
<https://www.hindawi.com>

